Rare-earth-doped nanophosphors for multicolor cathodoluminescence nanobioimaging using scanning transmission electron microscopy

Taichi Furukawa
Shoichiro Fukushima
Hirohiko Niioka
Naoki Yamamoto
Jun Miyake
Tsutomu Araki
Mamoru Hashimoto

Rare-earth-doped nanophosphors for multicolor cathodoluminescence nanobioimaging using scanning transmission electron microscopy

Taichi Furukawa,[a] Shoichiro Fukushima,[b] Hirohiko Niioka,[b,*] Naoki Yamamoto,[c] Jun Miyake,[b] Tsutomu Araki,[b] and Mamoru Hashimoto[b]
[a]Osaka University, Institute for NanoScience Design, 1-3 Machikaneyama, Toyonaka, Osaka 560-8531, Japan
[b]Osaka University, Graduate School of Engineering Science, Department of Mechanical Science and Bioengineering, 1-3 Machikaneyama, Toyonaka, Osaka 560-8531, Japan
[c]Tokyo Institute of Technology, Department of Physics, Oh-okayama, Meguro-ku, Tokyo 152-8551, Japan

Abstract. We describe rare-earth-doped nanophosphors (RE-NPs) for biological imaging using cathodoluminescence (CL) microscopy based on scanning transmission electron microscopy (STEM). We report the first demonstration of multicolor CL nanobioimaging using STEM with nanophosphors. The CL spectra of the synthesized nanophosphors (Y_2O_3:Eu, Y_2O_3:Tb) were sufficiently narrow to be distinguished. From CL images of RE-NPs on an elastic carbon-coated copper grid, the spatial resolution was beyond the diffraction limit of light. Y_2O_3:Tb and Y_2O_3:Eu RE-NPs showed a remarkable resistance against electron beam exposure even at high acceleration voltage (80 kV) and retained a CL intensity of more than 97% compared with the initial intensity for 1 min. In biological CL imaging with STEM, heavy-metal-stained cell sections containing the RE-NPs were prepared, and both the CL images of RE-NPs and cellular structures, such as mitochondria, were clearly observed from STEM images with high contrast. The cellular CL imaging using RE-NPs also had high spatial resolution even though heavy-metal-stained cells are normally regarded as highly scattering media. Moreover, since the RE-NPs exhibit photoluminescence (PL) excited by UV light, they are useful for multimodal correlative imaging using CL and PL. © *2015 Society of Photo-Optical Instrumentation Engineers (SPIE)* [DOI: 10.1117/1.JBO.20.5.056007]

1 Introduction

Light microscopy (LM) and electron microscopy (EM) are widely used cellular imaging methods. LM is a useful method for imaging biomolecules stained with fluorescent probes in the fields of biology and medicine. Staining with multiple fluorescent probes such as dyes,[1] quantum dots (QDs),[2,3] and fluorescent proteins[4,5] allows simultaneous visualization of the distributions of individual biomolecular species with different emission spectra, and imaging with multiple labeling provides information about biological molecular interactions. On the other hand, EM gives us fine structural information about cellular components, such as the membrane, mitochondria, and endoplasmic reticulum.

The spatial resolution of EM is higher than that of LM because the spot size of a focused electron beam is on the order of nanometers. Furthermore, EM allows us to observe a molecular species at nanoscale resolution through immunostaining with gold nanoparticles (GNPs).[6,7] More than one kind of molecular species can be identified by using GNPs of different sizes.[8–10] There is also a method capable of identifying different types of biomolecules by using the sizes and shapes of QDs.[11]

The spatial resolution achievable with LM is limited to submicrometer order by the diffraction limit of light,[12] and discrimination of different kinds of biomolecules using EM is still difficult because EM images are monochromatic, not color. These limitations of LM and EM hamper the detailed understanding of cellular functions in life processes, especially in the case of complex distributions of molecules.

Cathodoluminescence (CL) is one candidate that fills this functional gap between LM and EM. CL is the light emission from a material induced by accelerated electrons. The spatial resolution of CL microscopy reaches the nanometer scale because the spot size of an electron beam is on the order of nanometers, and the CL color depends on the material.[13] Therefore, by using suitable imaging probes, CL microscopy enables multicolor biological imaging with nanoscale spatial resolution. To exploit these benefits, we have previously reported biological CL imaging with rare-earth-doped nanophosphors (RE-NPs) based on a combined scanning electron microscopy–cathodoluminescence (SEM-CL) technique.[14,15] Several research groups have also studied SEM-CL imaging.[16–19] However, SEM-CL imaging has difficulty in imaging cellular structural information due to a low contrast image, even samples stained with heavy metals such as osmium and uranium.

The scanning transmission electron microscopy–cathodoluminescence (STEM-CL) method[20,21] is also a promising technique for realizing multicolor biological imaging with nanoscale spatial resolution. It is known that images of cellular structure (e.g., organelles, membranes, and macromolecules) obtained with

*Address all correspondence to: Hirohiko Niioka, E-mail: niioka@bpe.es.osaka-u.ac.jp

STEM using thin cell sections stained with heavy metals have high contrast. To reveal the detailed cellular functions at nanoscale resolution, simultaneous observation of both structural information and protein distributions is quite important. Furthermore, higher spatial resolution and higher contrast are obtained compared with SEM-CL because the acceleration voltage of STEM (80 to 200 kV) reduces the electron scattering volume compared with SEM (typical acceleration voltage: ~30 kV).

Here, we describe multicolor biological imaging using CL microscopy based on STEM, with Y_2O_3:Eu and Y_2O_3:Tb RE-NPs, which have high resistance against electron beam irradiation and narrow spectral bandwidth. Using these nanophosphors allows simultaneous cellular structural imaging by STEM and multicolor imaging by CL. In addition, multimodal imaging using LM is also demonstrated using the same nanophosphors. To the best of our knowledge, this is the first demonstration of an imaging technique in which RE-NPs are applied to CL biological imaging using STEM.

2 Imaging System

2.1 STEM-CL System

Our CL system based on an STEM instrument (JEM-2100F) is illustrated in Fig. 1. CL is collected by a parabolic mirror, forming parallel rays. The parallel rays exit the STEM instrument through a quartz window. The CL is focused onto a slit of a spectrometer (Andor, SR163, $f = 163$ mm, $F/3.6$) by a lens and is detected by an electron multiplying (EM)-CCD detector (Andor, DU920p-BU) for spectral imaging.

The electron beam is controlled via the beam scanning system of the transmission electron microscopy/STEM instrument using an external PC and is scanned on the specimen. CL from the specimen is obtained by the EM-CCD for a certain duration at each point. Using the EM-CCD detector, the emission spectrum is detected for each pixel, realizing spectral imaging at each wavelength. Since the STEM and CL signals are simultaneously obtained by the external PC and the electron beam is scanned step-by-step to observe these images, the position of each pixel in the STEM image is identical to that in the CL image.
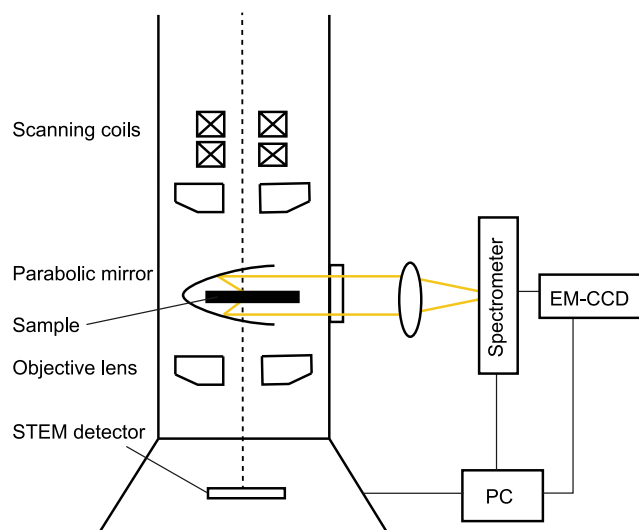
Fig. 1 Cathodoluminescence (CL) detection system combined with a scanning transmission electron microscopy (STEM) instrument.

2.2 Fluorescence Imaging System

For cellular fluorescence imaging using RE-NPs, we used an Hg-Ar lamp (Ocean Optics, CAL-2000) as a UV excitation light source. Only 254-nm UV light was used for the excitation light, by using a bandpass filter (Semrock, Hg-01-254). A UV objective lens (Nikon, UV50×A, NA = 0.4, WD = 11 mm) was used. Fluorescence bandpass filters were used for detection (for red emission: Semrock, FF01-615/20-25; for green emission: Semrock, FF01-550/32-25). The fluorescence was detected by an EM-CCD camera (Andor, Luca S).

3 Preparation of Specimens

3.1 Synthesis of RE-NPs

For the imaging probes, we used Y_2O_3:Eu and Y_2O_3:Tb RE-NPs. Y_2O_3-based RE-NPs are well-known materials for the application of CL to display devices and exhibit high intensity, narrow spectral bandwidth, and high stability against electron beam irradiation at acceleration voltages <30 Kv.[22] Y_2O_3:Eu and Y_2O_3:Tb NPs were synthesized using the homogeneous precipitation (HP) method.[23] The HP method is a nanophosphor synthesis method that produces nanophosphors of uniform size and spherical shape. Urea was used as the precipitant for homogeneous phosphor precursors. The precipitation reaction proceeds in the whole solution because the pH of the solution is increased by the hydrolysis reaction of urea into ammonia at about 80°C.

As the activator ions, Eu and Tb were selected for red and green phosphors, respectively. Rare-earth nitrates [$Y(NO_3)_3$, $Eu(NO_3)_3$ and $Tb(NO_3)_3$] were used as starting materials for the synthesis without further purification (all rare-earth nitrates were purchased from Kojundo Chemical Laboratory). The concentrations of Eu and Tb ions in the starting material solution were 5 mol % and 2 mol %, respectively, expressed as the concentrations of metal ions. Rare-earth nitrates were dissolved into 40 mL of distilled water to obtain a concentration of 4 mM. The solutions were stirred for 5 min. Urea (Wako Pure Chemical Industries, Ltd.) was added into the rare-earth nitrate solutions, and the solutions were stirred for 2 h at 80°C. Phosphor precursors started to precipitate in the solution derived from the hydrolysis reaction of urea. Finally, the obtained precursor nanoparticles and urea were separated by ultra-centrifugation (25,000 rpm, 10 min) performed three times and were annealed at 900°C for 1 h.

3.2 Cellular Specimens for STEM-CL Imaging and Fluorescence Imaging

Details of the specimen preparation for biological STEM-CL imaging and fluorescence imaging with HeLa cells are given here.

HeLa cells were cultured in Dulbecco's Modified Eagle Medium (DMEM) at 37°C in 5% CO_2. A distilled deionized water (DDW) solution that contained the two kinds of nanophosphors, Y_2O_3:Eu and Y_2O_3:Tb, was prepared at a concentration of 0.1 mg/mL (the concentrations of Y_2O_3:Eu and Y_2O_3:Tb were both 0.05 mg/mL). The nanophosphors in the solution were dispersed by ultrasound for 10 min. The 200 μL of the solution containing the dispersed nanophosphors was added to 2 mL DMEM solution in a cell culture dish, and the phosphors were introduced into the HeLa cells via endocytosis for 1 day.

The cells were fixed using 2.4% glutaraldehyde in 0.2 M Millonig's phosphate buffer at room temperature for 30 min. Postfixation was performed in 2% osmium tetroxide aqueous solution at 4°C for 1 h. After the fixation process, the specimen was rinsed three times in buffer solution. To enhance the membrane contrast for observation using STEM, samples were treated with 0.15% tannic acid in buffer solution for 1 min and immediately rinsed with the buffer and DDW. Poststaining was performed with 1% uranium acetate at 4°C for 1 h, and the specimens were washed. Dehydration was carried out with ethanol (30%, 50%, 70%, 80%, 90%, 95%, and 100% in triplicate, for 5 min at each concentration). The specimens were embedded in Quetol-821 epoxy resin (Nisshin EM) via the following process. The specimens were first treated with an ethanol–epoxy mixture (2:1 ethanol:epoxy resin) for 2 h, followed by treatment with an ethanol–epoxy mixture having a different concentration (1:2 ethanol:epoxy resin) for 12 h. The resin mixture was then replaced with fresh 100% resin, and the specimens were treated with this resin for 2 h. After this, the resin was again replaced with fresh 100% resin. The epoxy was then polymerized with the sequence: 45°C for 12 h → 60°C for 48 h → 45°C for 12 h. The epoxy molded samples were sliced to 100-nm thin sections using an ultramicrotome. The sliced thin section of the cell was placed on an elastic carbon-coated copper grid (Okenshoji Co., Ltd., SHR-C075 STEM Cu75P).

For fluorescence imaging, in the incubation process, cells were prepared in culture dishes with quartz windows at the bottom to allow the 254-nm UV light to pass through and to avoid background fluorescence from the window. The cells were fixed with 4% paraformaldehyde (Wako) after injection of the Y_2O_3 : Eu and Y_2O_3 : Tb nanophosphors, and the cells were observed using the fluorescence microscope described previously.

4 STEM-CL Imaging and Characterization of Y_2O_3 : Eu and Y_2O_3 : Tb Nanophosphors

First, we measured the CL spectra of the synthesized Y_2O_3 : Eu and Y_2O_3 : Tb nanophosphors on the elastic carbon-coated copper grids using the STEM-CL system in Fig. 1. Figure 2 shows normalized CL intensity spectra of Y_2O_3 : Eu (red) and Y_2O_3 : Tb (green) nanophosphors. The emission at around 600 nm from Eu^{3+} ions is due to the magnetic dipole transition $^5D_0 \Rightarrow$ $^7F_1$, which is insensitive to the symmetry of the lattice field, and the most intense emission around 615 nm is derived from the
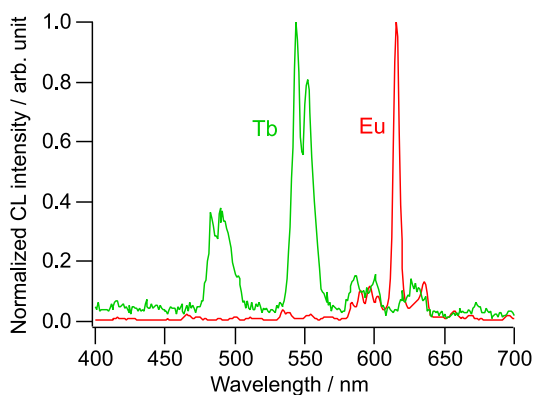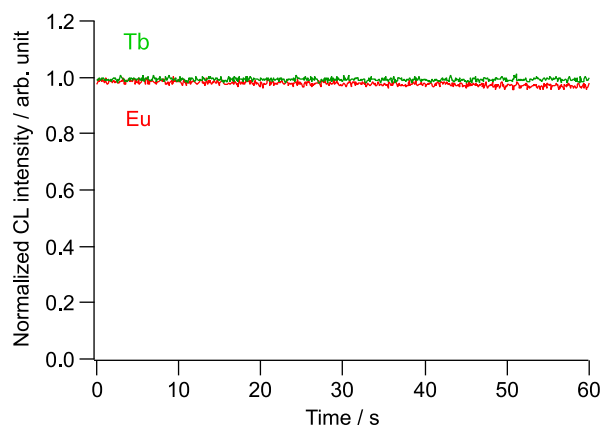
electric dipole transition $^5D_0 \Rightarrow {}^7F_2$.[22] In the Tb^{3+} ions, electric and magnetic dipole transitions are induced regardless of the symmetry of the lattice field, and the peak in the luminescence intensity is maximum around 545 nm ($^5D_4 \Rightarrow {}^7F_5$).[22] Since the most intense emission bands between Y_2O_3 : Eu and Y_2O_3 : Tb had almost no overlap and were very narrow, these two kinds of spectra are easy to distinguish.

In biological CL imaging, bleaching of probes due to high-energy electron exposure has been a crucial problem especially for organic fluorophors.[24] In inorganic materials, although QDs have high quantum efficiency and high resistance against light exposure,[25] they are easily bleached by electron beam exposure (data not shown). To confirm the stability under electron beam exposure, we examined the CL intensity of Y_2O_3 : Eu and Y_2O_3 : Tb as a function of time (Fig. 3). The electron beam was focused at one point on each phosphor, and the CL intensity was monitored. The acceleration voltage of the electrons was set to 80 kV. Intensity decreases of about 1% and 3% were observed for 60 s exposure in the Y_2O_3 : Eu and Y_2O_3 : Tb samples, respectively. The intensity decrease of the phosphors includes the effect of hydrocarbon contamination from the elastic carbon-supported copper grid and the epoxy resin, thus the actual intensity decay of these phosphors will be smaller.

The CL stability of these phosphors was high enough to achieve imaging even after long-term exposure with high acceleration voltage electrons. This suggests that Y_2O_3-based RE-NPs are suitable phosphors for biological CL imaging using the STEM-CL method. It is known that these types of phosphors are stable for low acceleration voltages (about 3 kV).[26] So far, use of these phosphors for biological measurement of CL intensity using a STEM-CL system has not been reported yet. Our experiments showed that these phosphors can also be used at high acceleration voltage (80 kV). Moreover, our results show the possibility of repeatable observation using STEM with multiple colors.

Figure 4 shows STEM and CL images of Y_2O_3 : Eu and Y_2O_3 : Tb nanophosphors. The two contacting particles were spatially resolved, indicating that the spatial resolution of the CL images was a few tens of nanometers, which is obviously beyond the diffraction limit of light. A possible reason for the high spatial resolution is the high acceleration voltage of this STEM system. Since a higher acceleration voltage prevents scattering of electrons in both the membrane and the phosphors, the excitation volume of CL is close to the size of the focused

Fig. 2 Spectra of Y_2O_3 : Tb and Y_2O_3 : Eu nanophosphors synthesized by homogeneous precipitation (HP) method (slit size: 0.1 nm, blaze wavelength: 400 nm, groove density: 150 L/mm).

Fig. 3 Stability of CL intensity against electron beam exposure (Y_2O_3 : Eu nanophosphors synthesized by homogeneous method).
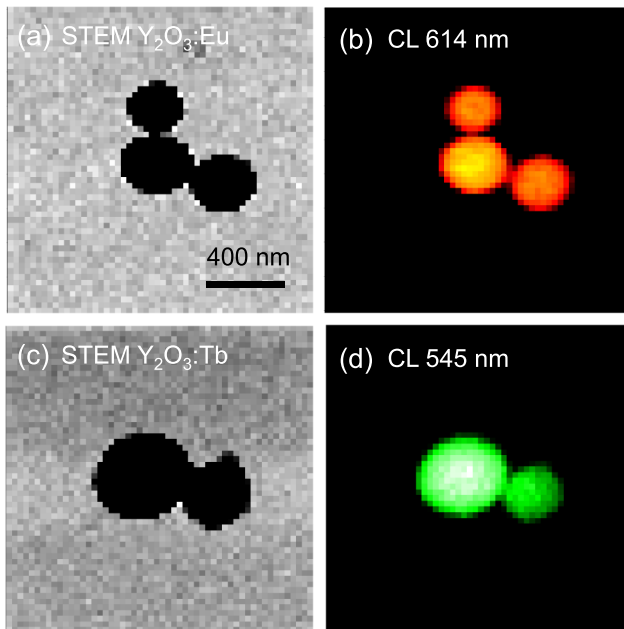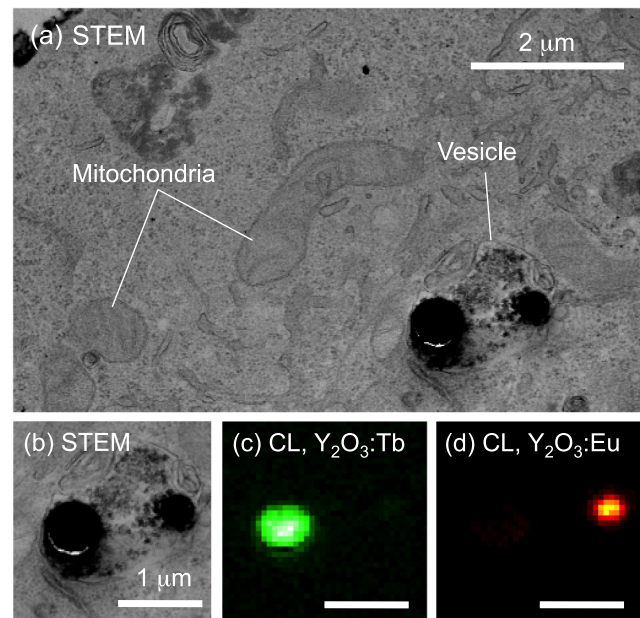
Fig. 4 STEM and CL images of Y_2O_3:Eu and Y_2O_3:Tb nanophosphors synthesized by HP method. (a) and (b) Interlaced STEM image and CL image of Y_2O_3:Eu. (c) and (d) Interlaced STEM image and CL image of Y_2O_3:Tb.

Fig. 5 STEM and CL images of Y_2O_3:Eu and Y_2O_3:Tb nanophosphors in 100 nm thin section of HeLa cell. (a) STEM image of 100 nm thin section of HeLa cell with introduced nanophosphors, (b) partial view of STEM image of HeLa cell with introduced nanophosphors, (c) and (d) CL images of nanophosphors (Y_2O_3:Eu and Y_2O_3:Tb) in a cell.

electron beam spot. The obtained CL images had high contrast compared with typical SEM-CL images because of the high CL intensity induced by the high acceleration voltage and the high beam current of the electron beam. The low scattering volume also gives high-contrast images since it prevents undesired CL from nonphosphor areas.[15] The aforementioned results demonstrate the suitability of these phosphors and our STEM-CL system for biological CL imaging.

5 Cellular STEM-CL and Fluorescence Imaging of HeLa Cells Using Y_2O_3:Eu and Y_2O_3:Tb Nanophosphors

We demonstrated multicolor biological STEM-CL imaging with nanoscale spatial resolution by using RE-NPs. Figure 5 shows STEM and color CL images of a HeLa cell containing Y_2O_3:Eu and Y_2O_3:Tb introduced by endocytosis. The acceleration voltage and current were 80 kV and 2 nA, and the exposure time for CL images was set to 100 ms/pixel. From the STEM image, nanophosphors were observed in the endocytotic vesicle, and mitochondria and nanophosphors were both clearly observed in the cell structure. The sizes of the introduced nanophosphors were 300 nm (Y_2O_3:Eu) and 500 nm (Y_2O_3:Tb). Although it was not possible to discriminate the two kinds of nanophosphors from the STEM image [Fig. 5(a)], the nanophosphor species could be identified from the CL spectra [Figs. 5(c) and 5(d)]. The spatial resolution of the CL images was beyond the diffraction limit of light.

Since the contrast of these CL images was similar to that of the CL images of phosphors dispersed on elastic carbon-coated copper grid [Figs. 4(b) and 4(d)], it was found that light obstruction due to the biological composition was negligible. In this multicolor biological imaging, crosstalk of the emission from Y_2O_3:Eu and Y_2O_3:Tb did not hinder discrimination of the phosphor emission. Although cellular regions stained with heavy metals (osmium and uranium) are considered to cause

scattering of the electron beam, almost no undesired CL due to scattering from the cellular region was observed in the CL images. The reason for this is the sufficiently high acceleration voltage and sufficiently thin cellular section. It is known that some types of proteins and lipids emit autofluorescence,[27–29] but such fluorescence did not affect the image contrast in this experiment. Since the CL signal from the cellular region was negligibly small, the contrast was maintained compared with CL images of phosphors dispersed on the elastic carbon-supported copper grid. These results imply that our biological STEM-CL imaging might be suitable for color EM. In recent years, synthesis of RE-NPs of 20 to 60 nm in diameter using the hydrothermal method has been reported.[30] It may be possible to apply methods of this kind to the synthesis of Y_2O_3:Eu and Y_2O_3:Tb nanophosphors.

It is possible to excite Y_2O_3-based RE-NPs with not only an electron beam but also UV light.[31] Thus, multimodal multiscale imaging using CL microscopy and fluorescence microscopy is possible using the same probes. Figure 6(a) shows photoluminescence spectra of Y_2O_3:Eu and Y_2O_3:Tb nanophosphors under 254-nm UV excitation. The inset shows a photograph of the photoluminescence. The shapes of the spectra are similar to those of the CL spectra, and the most intense peaks did not spectrally overlap. Figures 6(b) to 6(d) show transmission, photoluminescence, and merged (transmission, red fluorescence, and green fluorescence) images of a HeLa cell containing Y_2O_3:Eu and Y_2O_3:Tb. These nanophosphors were identified with their emission wavelengths. Although some aggregated phosphors were not resolved spatially, imaging of a large area in wet conditions was possible.

These nanophosphors can be used in correlative light and electron microscopy (CLEM). CLEM is one kind of bimodal imaging method for biological observation, which combines the advantages of both LM and EM.[32–34] The combination of
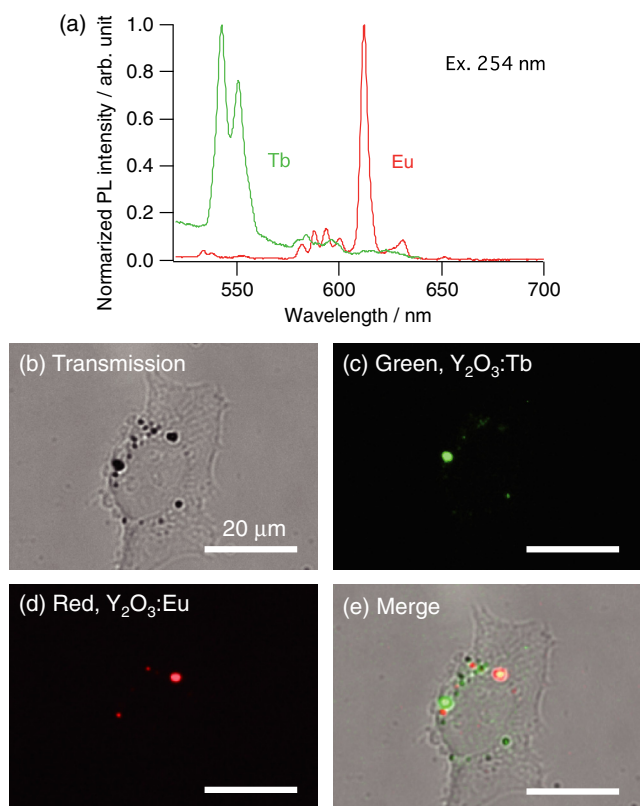
Fig. 6 (a) Emission spectra of Y_2O_3:Eu, Y_2O_3:Tb, (b) transmission, (c) green fluorescence, (d) red fluorescence, and (e) merged images of Y_2O_3:Eu and Y_2O_3:Tb nanophosphors contained in a HeLa cells. Y_2O_3:Eu, and Y_2O_3:Tb nanophosphors were excited by 254-nm UV light.

LM and EM offers more information about biological specimens than either method alone. However, in typical CLEM, multicycle observation of a thin-sectioned sample using LM and EM is not possible due to bleaching of fluorescence probes after irradiation with an electron beam. Our probes make it possible to store stained biological samples, like immunogold-stained samples, which can then be repeatedly used. In addition, fluorescence imaging in wet conditions makes it easy to check the sample condition before carrying out the time-consuming sample preparation process required for CL imaging (e.g., molding, sectioning).

For imaging with deeper penetration and less autofluorescence using LM, upconversion fluorescence imaging is an effective approach.[35,36] We have already proposed multimodal/correlative microscopy using Y_2O_3:Tm, Yb (thulium and ytterbium doped yttria) nanophosphors, which are excited by both an electron beam and near-infrared light.[37] This multimodal microscopy, allowing observation at different scales using LM and CL, may contribute to the discovery of new cellular and molecular functions and will improve the effectiveness of our imaging technique.

6 Summary

Multicolor high-resolution microscopy of biological specimens was performed using a STEM-CL system. CL images of Y_2O_3:Eu and Y_2O_3:Tb nanophosphors introduced into cells and heavy-metal-stained cellular structure were observed using the STEM-CL system. The CL spectra of the synthesized nanophosphors were sufficiently narrow to distinguish them from each other, and the spatial resolution of the CL images was sufficiently high to image biological molecules at a resolution beyond the diffraction limit of light. The Y_2O_3:Eu and Y_2O_3:Tb RE-NPs showed remarkable resistance against electron beam exposure even at a high acceleration voltage (80 kV) and kept a high CL intensity for 1 min. CL images of the RE-NPs nanophosphors in cells and the cellular structure, such as mitochondria and endocytotic vesicle, were clearly observed from the STEM image with high contrast. The spatial resolution of cellular CL imaging using RE-NPs was not reduced much, even though heavy-metal-stained cells are usually regarded as highly scattering media.

Y_2O_3:Eu and Y_2O_3:Tb RE-NPs will be useful phosphors for biological STEM-CL imaging at high spatial resolution beyond the diffraction limit of light, and the application of this immunostaining method will allow us to identify protein species at high spatial resolution with cellular structural information.

References

1. N. Panchuk-Voloshina et al., "Alexa dyes, a series of new fluorescent dyes that yield exceptionally bright, photostable conjugates," *J. Hystochem. Cytochem.* **47**(9), 1179–1188 (1999).
2. X. Michalet et al., "Quantum dots for live cells, in vivo imaging, and diagnostics," *Science* **307**(5709), 538–544 (2005).
3. V. M. Alexander, P. L. Choyke, and H. Kobayashi, "Fluorescent molecular imaging: Technical progress and current preclinical and clinical applications in urogynecologic diseases," *Curr. Mol. Med.* **13**(10), 1568–1578 (2013).
4. O. Shimomura, F. H. Johnson, and Y. Saiga, "Extraction, purification and properties of aequorin, a bioluminescent protein from the luminous hydromedusan, aequorea," *J. Cell. Comp. Physiol.* **59**, 223–239 (1962).
5. R. N. Day and M. W. Davidson, "The fluorescent protein palette: tools for cellular imaging," *Chem. Soc. Rev.* **38**, 2887–2921 (2009).
6. J. W. Stirling, "Immuno- and affinity probes for electron microscopy: a review of labeling and preparation techniques," *J. Histochem. Cytochem.* **38**(2), 145–157 (1990).
7. M. C. Risueno and P. S. Testillano, "Cytochemistry and immunocytochemistry of nucleolar chromatin in plants," *Micron* **25**(4), 331–360 (1994).
8. B. L. Wang and L. I. Larsson, "Simultaneous demonstration of multiple antigens by indirect immunofluorescence or immunogold staining. Novel light and electron microscopical double and triple staining method employing primary antibodies from the same species," *Histochemistry* **83**(1), 47–56 (1985).
9. R. S. Petralia et al., "Selective acquisition of AMPA receptors over postnatal development suggests a molecular basis for silent synapses," *Nat. Neurosci.* **2**(1), 31–36 (1999).
10. H. J. Geuze et al., "Use of colloidal gold particles in double-labeling immunoelectron microscopy of ultrathin frozen tissue sections," *J. Cell Biol.* **89**(3), 653–665 (1981).
11. B. N. G. Giepmans et al., "Correlated light and electron microscopic imaging of multiple endogenous proteins using quantum dots," *Nat. Methods* **2**, 743–749 (2005).
12. M. Born and E. Wolf, *Principles of Optics*, 6th ed., Cambridge, New York (1980).

13. B. G. Yacobi and D. B. Holt, *Cathodoluminescence Microscopy of Inorganic Solids*, Plenum, New York (1990).
14. H. Niioka et al., "Multicolor cathodoluminescence microscopy for biological imaging with nanophosphors," *Appl. Phys. Express* **4**, 112402 (2011).
15. T. Furukawa et al., "High-resolution microscopy for biological specimens via cathodoluminescence of Eu- and Zn-doped Y_2O_3 nanophosphors," *Opt. Express* **21**(22), 25655–25663 (2013).
16. E. Kimura et al., "Cathodoluminescence imaging for identifying uptaken fluorescence materials in Kupffer cells using scanning electron microscopy," *Arch. Histol. Cytol.* **67**(3), 263–270 (2004).
17. P. J. Fisher et al., "Enhanced biological cathodoluminescence," *Opt. Commun.* **281**, 1901–1908 (2008).
18. Y. Nawa et al., "Dynamic and high-resolution live cell imaging by direct electron beam excitation," *Opt. Express* **20**(5), 5629–5635 (2012).
19. D. R. Glenn et al., "Correlative light and electron microscopy using cathodoluminescence from nanoparticles with distinguishable colours," *Sci. Rep.* **2**, 865 (2012).
20. N. Yamamoto and K. Araya, "Photon emission from silver particles induced by a high-energy electron beam," *J. Phys. Rev. B* **64**, 205419 (2001).
21. N. Yamamoto, S. Ohtani, and F. J. G. de Abajo, "Gap and Mie plasmons in individual silver nanospheres near a silver surface," *Nano Lett.* **11**, 91–95 (2011).
22. W. M. Yen, S. Shionoya, and H. Yamamoto, *Phosphor Handbook*, CRC, Florida (2007).
23. N. Venkatachalam, Y. Saito, and K. Soga, "Synthesis of Er^{3+} doped Y_2O_3 nanophosphors," *J. Am. Ceram. Soc.* **92**(5), 1006–1010 (2009).
24. J. Niitsuma et al., "Cathodoluminescence investigation of organic materials," *J. Electron Microsc.* **54**, 325–330 (2005).
25. J. K. Jaiswal and S. M. Simon, "Potentials and pitfalls of fluorescent quantum dots for biological imaging," *Trends Cell Biol.* **14**(9), 497–504 (2004).
26. T. Nagata, T. Nakayama, and H. Murakami, "Low voltage cathodoluminescent properties of Y_2O_3-based nano-particle phosphors," in *SID'07 Digest*, pp. 1328–1331 (2007).
27. T. Ito et al., "Color cathodoluminescence images and cathodoluminescence spectra analysis of biological materials," *Acta Histochem. Cytochem.* **19**(5), 621–633 (1986).
28. T. Nakano et al., "Application of analytical color fluorescence electron microscopy to biomedical field: I. Vitamin A ester in rat retina," *Acta Histochem. Cytochem.* **23**(6), 753–767 (1990).
29. T. Nakano, H. Koike, and K. Ogawa, "Analytical color fluorescence electron microscopy of adrenal cortex," *Microsc. Res. Tech.* **36**, 454–462 (1997).
30. M. K. Devaraju, S. Yin, and T. Sato, "Tm^{3+}-doped Y_2O_3 nanocrystals: rapid hydrothermal synthesis and luminescence," *Eur. J. Inorg. Chem.* (29–30), 4441–4445 (2009).
31. R. Ozawa, "Photoluminescence of rare earth elements in Y_2O_3 and the application for their quantitative analysis," *Bunseki-kiki* **6**(2), 108–117 (1968) (in Japanese).
32. T. M. Svitkina and G. G. Borisy, "Correlative light and electron microscopy of the cytoskeleton of cultured cells," *Methods Enzymol.* **298**, 570–592 (1998).
33. T. M. Svitkina et al., "Mechanism of filopodia initiation by reorganization of a dendritic network," *J. Cell Biol.* **160**, 409–421 (2003).
34. C. Smith, "Two microscopes are better than one," *Nature* **492**, 293–297 (2012).
35. S. F. Lim et al., "In vivo and scanning electron microscopy imaging of upconverting nanophosphors in caenorhabditis elegans," *Nano Lett.* **6**(2), 169–174 (2006).
36. M. Nyk et al., "High contrast in vitro and in vivo photoluminescence bioimaging using near infrared to near infrared upconversion in Tm^{3+} and Yb^{3+} doped fluoride nanophosphors," *Nano Lett.* **8**(11), 3834–3838 (2008).
37. S. Fukushima et al., "Y_2O_3:Tm, Yb nanophosphors for correlative upconversion luminescence and cathodoluminescence imaging," *Micron* **67**, 90–95 (2014).

Biographies for the authors are not available.